How does horizontal diffusion influence the intensification and maximum intensity of numerically simulated tropical cyclones?

Rong Fei[a,b,c] and Yuqing Wang[c]

[a] *State Key Laboratory of Severe Weather, Chinese Academy of Meteorological Sciences, China Meteorological Administration, Beijing, China*

[b] *College of Earth and Planetary Sciences, University of Chinese Academy of Sciences, Beijing, China*

[c] *International Pacific Research Center and Department of Atmospheric Sciences, School of Ocean and Earth Science and Technology, University of Hawaii at Manoa, Honolulu, HI, USA*

January 13, 2022 (submitted)

July 13, 2022 (first revision)

October 28, 2022 (second revision)

Dateline

Submitted to ***Journal of the Atmospheric Sciences***

Corresponding author: Yuqing Wang, yuqing@hawaii.edu

ABSTRACT

Recent studies have demonstrated the sensitivity of simulated tropical cyclone (TC) intensity to horizontal diffusion in numerical models. It is unclear whether such sensitivity comes from the horizontal diffusion in or above the boundary layer. To address this issue, both an Ooyama-type model and a full-physics model are used to conduct sensitivity experiments with reduced or enlarged horizontal mixing length (l_h) in the boundary layer and/or in the free atmosphere. Results from both models show that enlarging (reducing) l_h throughout the model domain considerably reduces (increases) the TC intensification rate and quasi-steady intensity. A new finding is that changing l_h above the boundary layer imposes a much greater influence than that in the boundary layer. Large l_h above the boundary layer is found to effectively reduce the radial gradient of tangential wind inside the radius of maximum tangential wind and thus the inward flux of absolute vorticity, reducing the positive tangential wind tendency and the TC intensification rate and the steady-state intensity. In contrast, although larger l_h in the boundary layer reduces the boundary-layer tangential wind tendency, it also leads to the more inward-penetrated inflow and thus enhances the inward flux of absolute vorticity, which offsets part of the direct negative contribution by horizontal diffusion, making the net change in tangential wind tendency not obvious. Results from three-dimensional simulations also show that the resolved eddies contribute negatively to TC spinup when l_h is small, while its effect weakens when l_h is enhanced either in or above the boundary layer.

1. Introduction

Turbulent mixing processes are of great importance to the intensification and maintenance of tropical cyclones (TCs), especially the turbulences within the boundary layer and near the eyewall (Emanuel 1995, 1997; Bryan and Rotunno 2009a,b, hereafter BR09a,b; Rotunno et al. 2009; Rotunno and Bryan 2012, hereafter RB12; Zhang et al. 2015). This is because turbulence mixes dynamic and thermodynamic quantities both horizontally and vertically. In the conventional view, turbulent processes more specifically refer to the vertical turbulent mixing assuming that the horizontal counterpart is much smaller. This is why numerous efforts have been given to the vertical turbulent mixing in theoretical studies relevant to TC dynamics and the representation of vertical turbulent mixing in numerical models for improving TC forecasts. For example, in the classic Ekman spiral model of the boundary layer wind in a TC-like circular vortex, only the vertical turbulent transport of

momentum is considered without the inclusion of horizontal mixing (Eliassen 1971; Eliassen and Lystad 1977; Kepert 2001). Previous studies also demonstrated the sensitivity of the simulated TC structure and intensity to the representation of boundary layer turbulent mixing in numerical models (Braun and Tao 2000; Nolan et al. 2009a,b; Gopalakrishnan et al. 2013; Zhang et al. 2015). More recently, observational studies have also focused on quantifying the vertical mixing length in TC boundary layer (Zhang et al. 2011; Zhang and Drennan 2012).

Although the horizontal turbulent mixing is much smaller than the vertical mixing in TC boundary layer (Kepert and Wang 2001) and has received less attention in earlier studies on TC dynamics and modeling (Emanuel 1986), it is indispensable in all numerical weather and climate models. The horizontal turbulence parameterization plays three main roles in TC simulations. First, the small-scale turbulence (and also organized eddies) that cannot be explicitly resolved by the model resolution should be represented and parameterized using the resolve-scale motions. Second, horizonal diffusion is often used to prevent the formation of frontal discontinuities near the eyewall, and numerical instability (RB12). Third, in an axisymmetric TC model, the parameterized horizontal mixing also takes into account for non-axisymmetric eddy motions in affecting the azimuthal mean flow.

Recently, increasing effort has been devoted to understanding the effect of horizontal turbulent mixing on TC structure and intensity (Zhang and Montgomery 2012; Zhang and Marks 2015; Zhang et al. 2018; Wang et al. 2021). Horizontal diffusion is found essential to the intensity of numerically simulated TCs (BR09a,b; Bryan 2012). Using an axisymmetric numerical model, BR09a found a strong dependence of the simulated TC steady-state structure and intensity on the parameterized horizontal mixing length. Similar strong sensitivities of simulated TCs to horizontal mixing are also demonstrated in later axisymmetric (Bryan 2012; Tao et al. 2020) and three-dimensional numerical simulations (Zhang and Marks 2015). Zhang and Marks (2015) revealed the negative correlation between horizontal mixing length and TC intensification rate. Some efforts have also been made to tune the parameterization of horizontal diffusion in numerical models with the results showing some improvements to TC intensity forecasts (Zhang et al. 2018; Wang et al. 2021).

The sensitivity of the simulated TC maximum intensity to horizontal mixing length in axisymmetric simulations was explained by BR09a in terms of the modification to TC structure. They suggested that lateral mixing reduces the radial gradient of momentum so that the inward transport of angular momentum from the near-core environment into the TC inner core in the boundary layer could be reduced. A similar explanation was given in a three-

dimensional simulation by Zhang and Marks (2015). To understand the dynamics, RB12 conducted an angular momentum budget for the model output from idealized simulations. They found that horizontal diffusion contributes largely to the angular momentum budget in the inner-core boundary layer and acts to diffuse the radial distribution of angular momentum carried upward in the eyewall, producing a smaller maximum TC intensity.

Previous studies have attributed the dependence of the numerically simulated TC intensification and maximum intensity on horizontal mixing length (and thus horizontal diffusion) to the dynamical effect in TC boundary layer. Since most studies used a single horizontal mixing length throughout the model atmosphere, the sensitivity includes contributions by the horizontal diffusion in both the boundary layer and the free troposphere. Therefore, it is unclear whether and to what extent the horizontal diffusion above the boundary layer contributed to the sensitivity in previous studies. In this regard, the following two aspects should be considered. On the one hand, the TC eyewall has a frontogenetical nature with large radial gradients of key dynamical variables across the eyewall from the surface to the upper troposphere (Emanuel 1997). As a result, the lateral diffusion in the eyewall region is still noticeable above the boundary layer where the vertical turbulent mixing generally becomes small. On the other hand, the interior flow (mainly the gradient wind or pressure gradient force) in the free atmosphere largely controls the structure and intensity of the flow in the boundary layer (Kepert 2001; Kepert and Wang 2001; Li and Wang 2021a,b). This suggests that horizontal diffusion above the boundary layer may not only weaken the radial gradient of momentum locally but also modify the boundary-layer flow below, which may indirectly affect the TC intensification and maximum intensity by modifying the eyewall ascent and thus convection.

Considering the fact that there has been no study in the literature that has devoted to understanding the relative importance/contributions of horizontal diffusion in the boundary layer and in the free atmosphere to TC intensification and maximum intensity, we attempt to address this issue in this study based on sensitivity experiments using both the newly developed Ooyama-type three-layer TC model with a multilevel boundary layer by Fei and Wang (2021, thereafter FW21) and the widely used cloud model CM1 developed by BR09a. By specifying different values for horizontal mixing length in the boundary layer and in the free atmosphere in numerical simulations and performing tangential wind budget analysis, we can quantify and understand the relative importance of horizontal diffusions in and above the boundary layer to TC intensification and maximum intensity. The rest of the paper is

organized as follows. Section 2 describes model settings and experimental design. Results from the Ooyama-type TC model and those from the full-physics model CM1 are discussed in sections 3 and 4, respectively. Section 5 provides a summary of main conclusions and some further discussions.

2. Model and experimental design

Two numerical models are utilized to conduct a series of numerical experiments in this study. One is the improved version of the axisymmetric Ooyama-type three-layer TC model with a multilevel boundary layer (hereafter, OMBL model; FW21). Compared with the original Ooyama model (Ooyama 1969), in this version, the gradient wind balance assumption is removed and the original slab boundary layer is replaced with a multilevel boundary layer. The advantage of this succinct model is that modifications to the horizontal mixing length can be made independently in the boundary layer and in the free atmosphere above so that the relative contributions of horizontal diffusion in the two parts of the atmosphere can be quantified without any ambiguity. The other model is the full-physics cloud model—CM1 (BR09a), which is extensively used in idealized TC simulations to understand various aspects of TC dynamics (BR09a,b; Bryan 2012; Li et al. 2019, 2020). Note that although the simple OMBL model has its advantage to be used to address the issue under concern, the more sophisticated full-physics model CM1, which comprises comprehensive physical processes, can be used to confirm the robustness of conclusions obtained based on the simple model. The two models and the corresponding experimental designs are briefly described below.

a. The OMBL model

The governing equations, physical parameterizations, and model parameters of the Ooyama-type TC model (OMBL model) used in this study was elaborated by FW21 (see their section 2 for details). In brief, the OMBL model is composed of two layers of the free atmosphere formulated with shallow water equations of different densities and a multilevel boundary layer similar to that used in Kepert and Wang (2001) and Li and Wang (2021a,b). For clarity, layer b, layer 1, and layer 2 are used to refer to the boundary layer, the lower free troposphere, and the upper free troposphere, respectively. Exchanges of mass, momentum, and heat are allowed between different layers, and also exchanges of enthalpy and momentum between the boundary layer and the underlying ocean surface. The model has a

uniform radial grid spacing of 1 km, extending from the TC center outward to 2400 km, where an open lateral boundary condition is assumed. There are 20 vertical levels within the boundary layer with the top at 1774 m. Most model parameters are the same as those listed in Table 1 of FW21 except for those modified in accordance with the configurations of CM1 described in the next subsection. Specifically, the Coriolis parameter f is set to 5×10^{-5} s^{-1} (assumed at 20°N); Sea surface temperature (SST) is fixed at 29 ℃; The surface drag coefficient C_D is a function of wind speed and given as $10^{-3} \times \max\{1.0, \min[2.4, 1.0 + 0.07(|\overrightarrow{V_s}| - 5)]\}$, where $|\overrightarrow{V_s}|$ is the near-surface wind speed (Donelan 2004); The surface exchange coefficient C_E is a constant of 1.2×10^{-3} (Drennan et al. 2007). The subgrid-scale turbulent mixing is parameterized with the Smagorinsky-type scheme as used in CM1, with the horizontal turbulent diffusivity given as $K_h = {l_h}^2 \left[2(\frac{\partial u}{\partial r})^2 + 2\left(\frac{u}{r}\right)^2 + (\frac{\partial v}{\partial r} - \frac{v}{r})^2\right]^{1/2}$, where u, v are radial and tangential winds, respectively, r is radius, and l_h is the horizontal mixing length, which is set to be 700 m as default in control simulations (see section 2c below). The asymptotic vertical mixing length l_∞ in calculating vertical turbulent diffusivity is set to 70 m. These values are recommended by Bryan (2012) based on numerous axisymmetric TC simulations.

b. The CM1 model

The full-physics model used in this study is the nonhydrostatic and fully compressible cloud model CM1, version 19.10 (BR09a), and both axisymmetric and three-dimensional versions were utilized. The model domain is 3100 km in radius (or in x and y directions for three-dimensional simulations) and 25 km in the vertical direction. The horizontal grid spacing is 1 km in the inner core and stretched to 14 km to the radial outer boundary. The model has 59 vertical levels with fixed grid spacing of 0.5 km above 5.5 km and compressed grids below. Cloud/precipitation processes are parameterized with the double-moment microphysics scheme of Thompson et al. (2008) and no cumulus convective parameterization is used in all simulations. To mimic radiative cooling, Newtonian cooling capped at 2 K day^{-1} is added to the thermodynamic equation (Rotunno and Emanuel 1987). The parameterization of subgrid-scale turbulent mixing also follows the Smagorinsky-type scheme, as introduced in BR09a, with the default asymptotic vertical mixing length and horizontal mixing length of 70 m and 700 m, respectively, as in the default OMBL model. The surface exchange coefficients for momentum and heat are the same as those in OMBL model (section 2a). An f

plane is assumed with the Coriolis parameter of 5×10^{-5} s^{-1} and SST is set constant at 29°C. The unperturbed environment of the model atmosphere adopts the moist tropical sounding of Dunion (2011). In general, the vertical and horizontal mixing parameterizations and the relevant parameters, as well as the surface drag and exchange coefficients, in CM1 and OMBL are identical. This makes it feasible to examine the consistency of the sensitivity of the simulated TC structure and intensity to changes in the horizontal mixing length in the two models.

c. Experimental design

The initial cyclonic vortex in both OMBL and CM1 models has the same radial distribution of tangential wind following Wood and White (2011), with the initial maximum tangential wind speed of 15 m s^{-1} at a radius of 80 km from the TC center and with the radial decaying parameter of 1.6. In OMBL simulations, the initial vortex is specified in the boundary layer and in the lower layer of the free troposphere while there is no flow in the upper layer of the free atmosphere. The initial tangential wind in CM1 simulations decreases linearly with height from the maximum 15 m s^{-1} at the surface to zero at a height of about 18 km. In addition, to reduce the internal variability in CM1 axisymmetric simulations and gain robust model results, ensemble simulations with 21 members are performed, as done in Li et al. (2020). Namely, in addition to the standard run described above, in the remaining 20 runs, the initial maximum tangential wind speed is perturbed by increments of $\pm$0.1 m s^{-1} (for 10 runs), and the initial radius of maximum tangential wind (RMW) is perturbed by increments of $\pm$0.4 km (for 10 runs). All simulations in OMBL and CM1 models are integrated for 192 h when TCs achieve their quasi-steady stages in all simulations.

A series of numerical experiments were performed to quantify the relative importance of horizontal diffusions in the boundary and in the free atmosphere to the simulated TC intensification and maximum intensity (Table 1). In the control experiment of OMBL (O-CTL), all default model settings described in section 2a were employed. In two sets of OMBL sensitivity experiments, the horizontal turbulent mixing was enhanced and reduced, respectively. Specifically, in the first set of five experiments, the horizontal mixing length (l_h) was reduced to 300 m (in contrast to 700 m in O-CTL) in the whole model domain (O-ALL-300), in layers 1 and 2 (O-F12-300), in layer b (O-B-300), in layer 1 (O-F1-300), and in layer 2 (O-F2-300), respectively. In the second set of five experiments, l_h was enlarged to

206 1500 m in the whole model domain (O-ALL-1500), in layers 1 and 2 (O-F12-1500), in layer
207 b (O-B-1500), in layer 1 (O-F1-1500), and in layer 2 (O-F2-1500), respectively.

208 Table 1. List of numerical experiments.

Exp.	Model	Horizontal diffusion
O-CTL	OMBL	Default in OMBL (l_h = 700 m)
O-ALL-300 (1500)	OMBL	l_h = 300 m (1500 m) in the whole domain
O-B-300 (1500)	OMBL	l_h = 300 m (1500 m) in layer b
O-F12-300 (1500)	OMBL	l_h = 300 m (1500 m) in layer 1 and 2
O-F1-300 (1500)	OMBL	l_h = 300 m (1500 m) in layer 1
O-F2-300 (1500)	OMBL	l_h= 300 m (1500 m) in layer 2
C-CTL	CM1	Default in CM1 (l_h = 700 m)
C-ALL-300 (1500)	CM1	l_h = 300 m (1500 m) in the whole domain
C-z1.5-300 (1500)	CM1	l_h = 300 m (1500 m) if z $\leqslant$ 1.5 km
C-z1.5-10-300 (1500)	CM1	l_h = 300 m (1500 m) if 1.5 < z < 10 km
C-lz10-300 (1500)	CM1	l_h = 300 m (1500 m) if z $\geqslant$ 10 km

209 In CM1 simulations, the control experiment (C-CTL) used the default settings as
210 introduced in section 2b. Similar to the sensitivity experiments in OMBL, l_h was also
211 modified separately in CM1. The vertical domain was divided into three layers: the layer
212 below 1.5 km (boundary layer), the layer between 1.5 and 10 km (middle layer), and the layer
213 above 10 km (outflow layer). In the first set of CM1 experiments, l_h was reduced to 300 m in
214 the boundary layer (C-z1.5-300), middle layer (C-z1.5-10-300), outflow layer (C-lz10-300),
215 and throughout the model domain (C-ALL-300), respectively. Similarly, the sensitivity
216 experiments with l_h enlarged to 1500 m were labelled as C-z1.5-1500, C-z1.5-10-1500, C-
217 lz10-1500, and C-ALL-1500, respectively. The three layers were chosen based on the radial
218 wind structure of the simulated TC in C-CTL. Results from preliminary tests show that
219 changing the interfaces up or down by 0.5 km does not affect the major results discussed
220 below (not shown). Note that the use of extremely weak horizontal turbulent mixing (such as
221 the inviscid limit l_h= 0) would be unrealistic because in an axisymmetric model, the
222 horizontal diffusion represents the lateral mixing not only by the subgrid-scale axisymmetric
223 turbulence but also by the unresolvable asymmetric eddies. Since our focus is on the relative
224 importance of horizontal diffusions in the boundary layer and in the free atmosphere to TC
225 intensification and maximum intensity, we did not attempt to examine the whole parameter
226 space in this study but with those parameters chosen as previously suggested for TC
227 simulations.

228 ## 3. Results from OMBL simulations

Figure 1 presents the time series of TC intensities in terms of the maximum tangential winds in layer 1 (v_{1m}) and the 24-h intensity changes in OMBL simulations. Note that in OMBL, the tangential wind in layer 1 (v_1) is usually deemed as the interior flow and the maximum v_1 is often referred to as TC intensity (Ooyama 1969; FW21). The near-surface tangential wind shows consistent evolution with v_1 except for the systematically smaller values (not shown). We can see from Fig. 1 that the suppressed (enhanced) horizontal diffusion by reducing (enlarging) the horizontal mixing length in the whole model domain substantially accelerates (slows down) TC intensification (Figs. 1c,d) and leads to an increased (a decreased) quasi-steady intensity relative to those in the control OMBL experiment (O-CTL) (Figs. 1a,b), which agrees with the results reported in previous studies (e.g., BR09a; Zhang and Marks 2015).

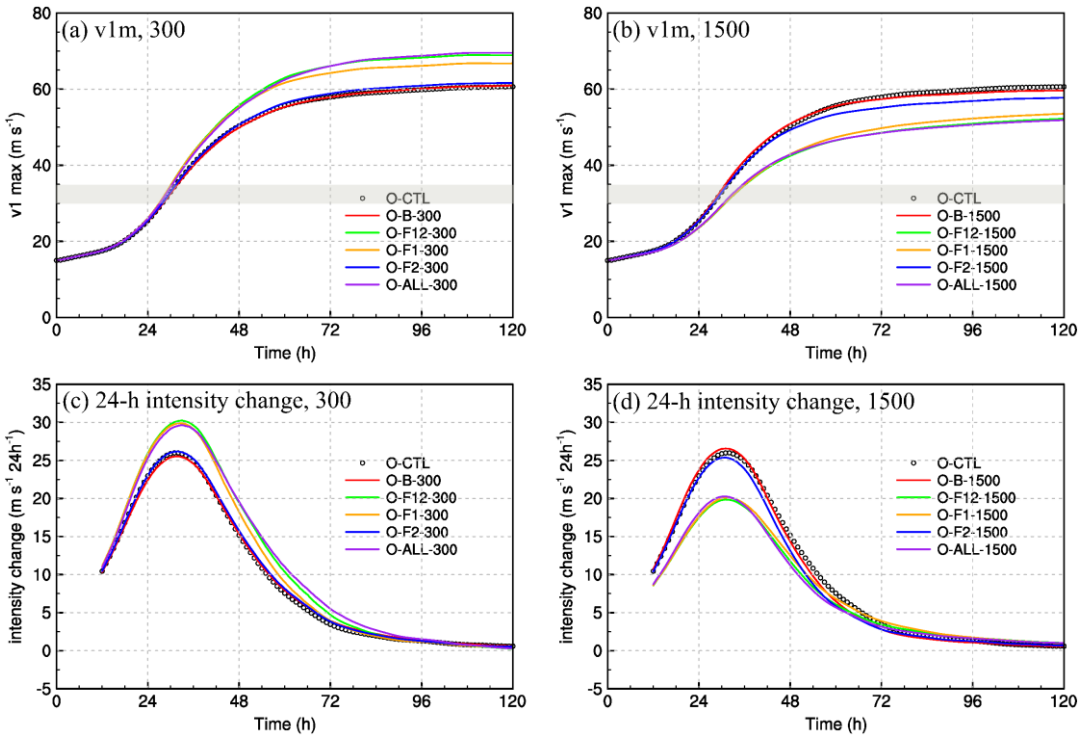

Figure 1. Time series of the simulated (a,b) maximum layer-1 tangential wind v_1 (v_{1m}; unit: m s^{-1}) and (c,d) intensification rate (unit: m s^{-1} 24h^{-1}) in OMBL model simulations. The left panels present the results with the horizontal mixing length reduced to 300 m. Black circles, red, green, orange, blue, and purple cures refer to O-CTL, O-B-300, O-F12-300, O-F1-300, O-F2-300, and O-ALL-300, respectively. The right panels are the same as the left panels but for experiments with the horizontal mixing length enlarged to 1500 m. The gray zones in (a) and (b) denote the period when v_{1m} increases from 30 to 35 m s^{-1}. Some further analyses about this intensifying period are conducted as shown in Figs. 3 and 4.

The reduced (enlarged) horizontal mixing length in the lower-layer free troposphere in O-F1-300 (O-F1-1500) leads to the increased (decreased) intensification rate and stronger

(weaker) quasi-steady intensity, which is comparable to the results with the reduced (enlarged) horizontal mixing length throughout the model atmosphere in O-ALL-300 (O-ALL-1500). In sharp contrast, modifications to the horizontal mixing length in either the boundary layer (O-B-300 and O-B-1500) or the upper-layer free troposphere (O-F2-300 and O-F2-1500) have negligible effects on both the TC intensification rate and the quasi-steady intensity. Note that the differences in TC intensity evolution and intensification rate among all experiments are not prominent until 24 h of the simulations (Fig. 1) because the disparity of horizontal diffusion among experiments becomes distinct with the increasing TC intensity (Fig. 2b). Nevertheless, the above results demonstrate that it is the horizontal diffusion in layer 1 immediately above the boundary layer that dominates the effect of horizontal diffusion on the simulated TC intensification rate and steady-state intensity, while the effects of horizontal diffusion in the boundary layer and in the upper troposphere are secondary.

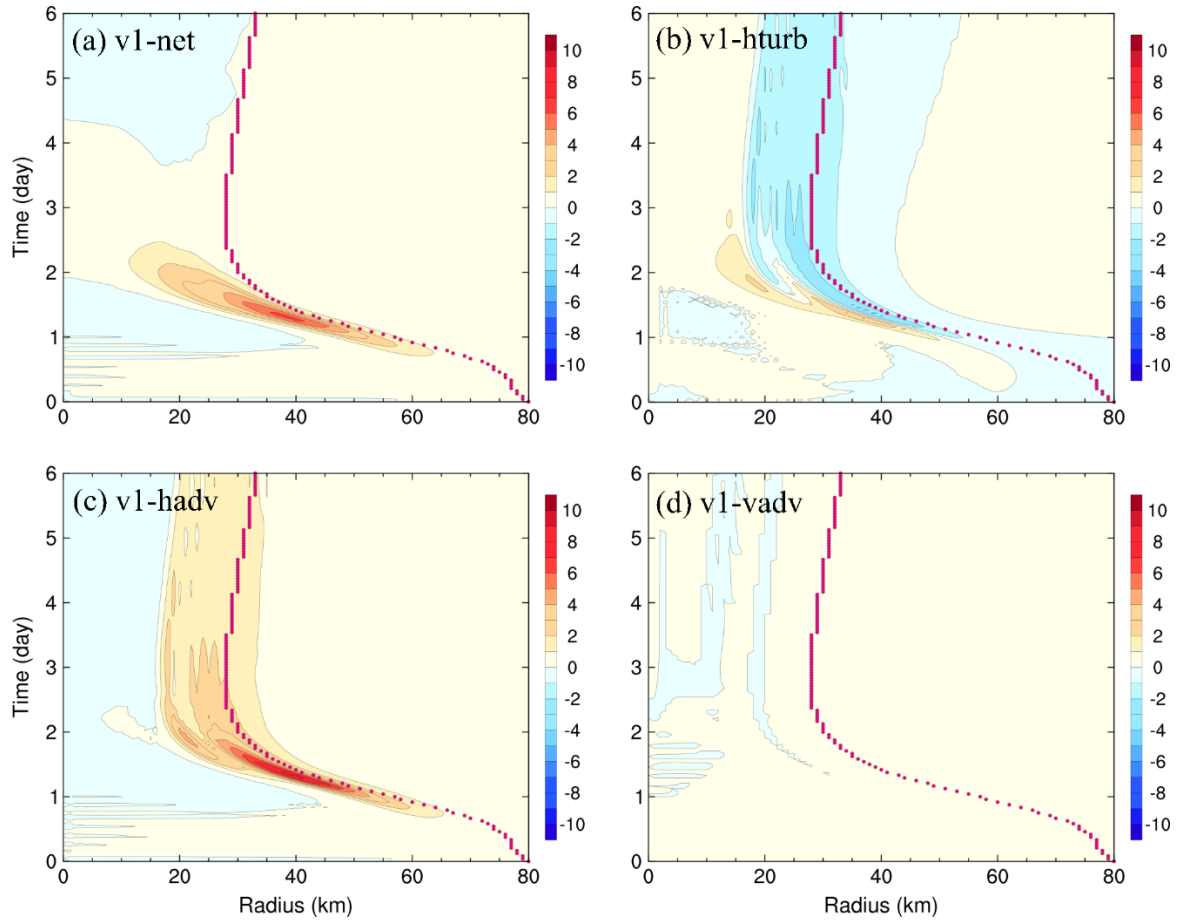

Figure 2. Radius-time diagrams of tendency terms (unit: m s^{-1} h^{-1}) of v_1 in O-CTL, including (a) the net tendency (v1-net), (b) horizontal diffusion (v1-hturb), (c) radial flux of absolute vorticity (v1-hadv), and (d) vertical advection (v1-vadv). Deep pink dots denote the radius of maximum v_1 (rmv_1).

To understand the above differences, the tangential wind budget analysis is performed for the lower-layer free troposphere. The tendency equation of tangential wind in layer 1 (v_1) in OMBL is given as

$$\frac{\partial v_1}{\partial t} = -u_1\zeta_{a1} + D_{v,v_1} + D_{hd,v_1}, \quad (1)$$

where $\zeta_{a1} = f + \frac{v_1}{r} + \frac{\partial v_1}{\partial r}$ is the absolute vertical vorticity. The term on the left-hand side is the local tendency of v_1 (v_1-net). Terms on the right-hand side refer to the tendencies of v_1 induced by, respectively, the radial flux of absolute vorticity (v_1-hadv), the upward advection of tangential wind from the boundary layer below (v_1-vadv[1]), and the horizontal diffusion of tangential wind (v_1-hturb[2]). Figure 2 shows the time evolution of radial distributions of all tendency terms in O-CTL. The local v_1 tendency (v_1-net) keeps positive near the radius of maximum v_1 (rmv_1, Fig. 2a) and always peaks inside of the rmv_1, contributing to the TC intensification and the contraction of the rmv_1 (Stern et al. 2015; Li et al. 2021). The inward flux of absolute vorticity (v_1-hadv) is the most significant contributor to TC intensification (Fig. 2c). The lateral turbulent mixing of v_1 (v_1-hturb), which acts to diffuse the peak of v_1 near the rmv_1, has an adverse effect on the local tendency of v_1 near the rmv_1, especially during the late intensification and quasi-steady stages (Fig. 2b). The negative value of horizontal diffusion near the rmv_1 increases progressively as TC intensifies because the horizontal diffusivity and the corresponding horizontal diffusion are both proportional to the radial gradient of v_1. The positive values of horizontal diffusion in the eye region inside the negative values indicate the inward mixing of high angular momentum to spin up the tangential wind in the eye region at the expense of reducing the positive tangential wind tendency near and immediately inside the rmv_1. Namely, horizontal diffusion has a negative impact on TC intensification. The tendency due to the upward momentum transport from the boundary layer is rather small. This is because most mass brought upward by updraft from the boundary layer is transported to the upper layer of the free troposphere during the intensification stage in the Ooyama-type model.

[1] The upward advection of tangential wind $D_{v,v_1} = Q_{b,1}\frac{v_b - v_1}{h_1}$, where v_b and v_1 are the tangential winds at the boundary-layer top and layer 1, respectively, h_1 is the depth of layer 1, $Q_{b,1}$ is a variable denoting the convection type and intensity and it is related with frictional updraft and thermodynamical stability. See section 2 of FW21 for more details.

[2] Horizontal diffusion of tangential wind $D_{hd,v_1} = \frac{1}{h_1 r^2}\frac{\partial}{\partial r}\left[K_h h_1 r^3 \frac{\partial}{\partial r}\left(\frac{v_1}{r}\right)\right]$.

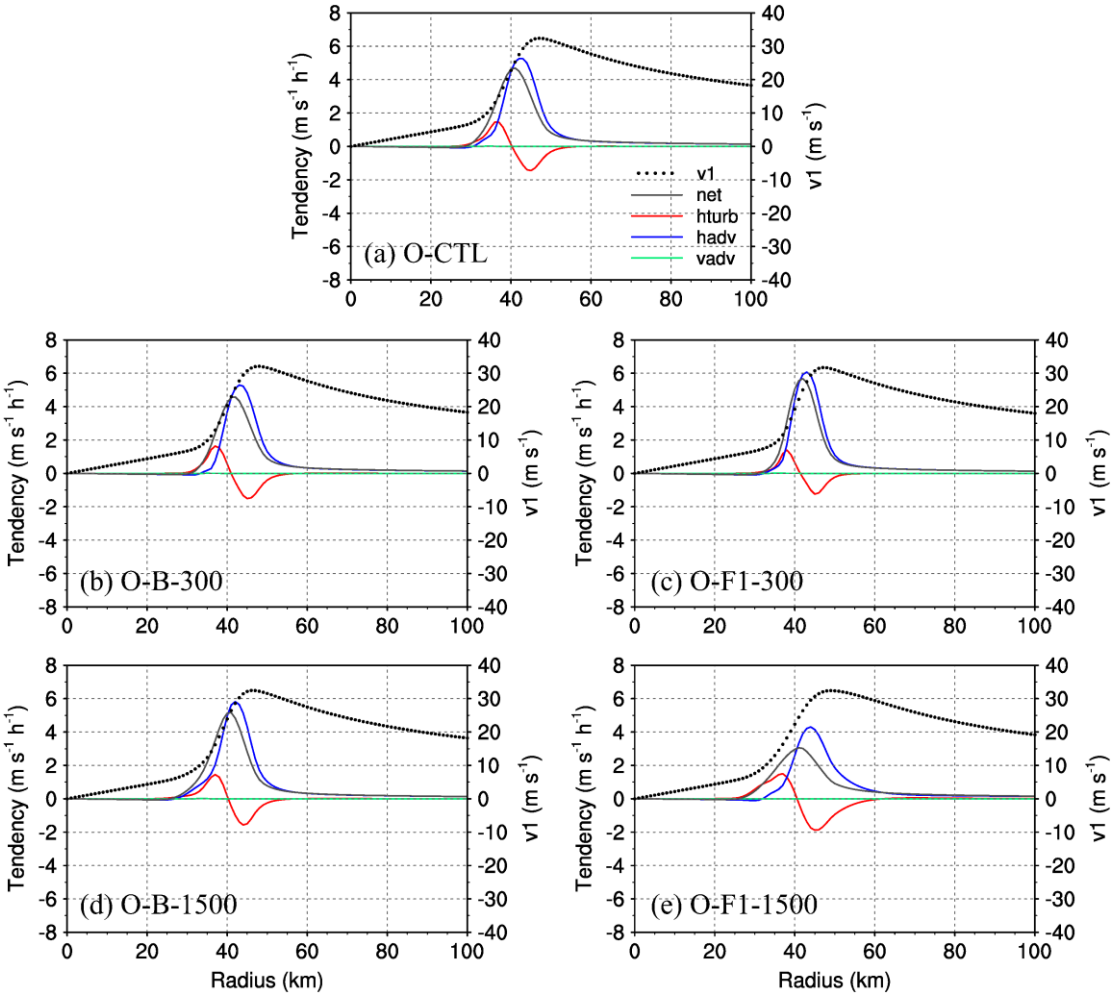

Figure 3. Radial profiles of v_1 (dots; right ordinate) and its tendency terms (curves; left ordinate) in (a) O-CTL, (b) O-B-300, (c) O-F1-300, (d) O-B-1500, and (e) O-F1-1500 during the period when v_{1m} increases from 30 to 35 m s^{-1}. Tendency terms include the net tendency (gray), horizontal diffusion of tangential wind (red), radial flux of absolute vorticity (blue), and vertical advection (green).

The radial profiles of v_1 and its tendency terms averaged during the periods when the TCs intensify from 30 to 35 m s^{-1} (marked in Fig. 1 with gray region) in O-CTL, O-B-300, O-B-1500, O-F1-300, and O-F1-1500 are compared in Fig. 3. The average TC intensities during the chosen periods among these experiments are similar so that the differences in tendency terms are not caused by the differences in the simulated TC intensities, making a fair comparison of tendency terms among these experiments. Note that results from O-F2-300 (O-F2-1500), O-F12-300 (O-F12-1500), and O-ALL-300 (O-ALL-1500) are similar to those in O-B-300 (O-B-1500) and O-F1-300 (O-F1-1500), respectively, and thus are not shown. Consistent with the results in O-CTL shown in Fig. 2, the net v_1 tendency near the rmv$_1$ is predominantly contributed by the radial flux of absolute vorticity, and the lateral diffusion spins up the tangential wind in the eye region but spins down the tangential wind near the

rmv$_1$ (Fig. 3a). Enlarging (reducing) the horizontal mixing length in the boundary layer makes little difference to the radial distributions of v_1 and its tendency terms (Figs. 3b,d). On the contrary, changing the horizontal mixing length in the lower-layer free troposphere largely modifies the v_1 tendency terms (Figs. 3c,e). The absolute value of the negative tendency due to horizontal diffusion near the rmv$_1$ is reduced in O-F1-300 while the positive inward flux of absolute vorticity is increased, together giving rise to larger positive net tendency of v_1 and thus larger TC intensification rate.

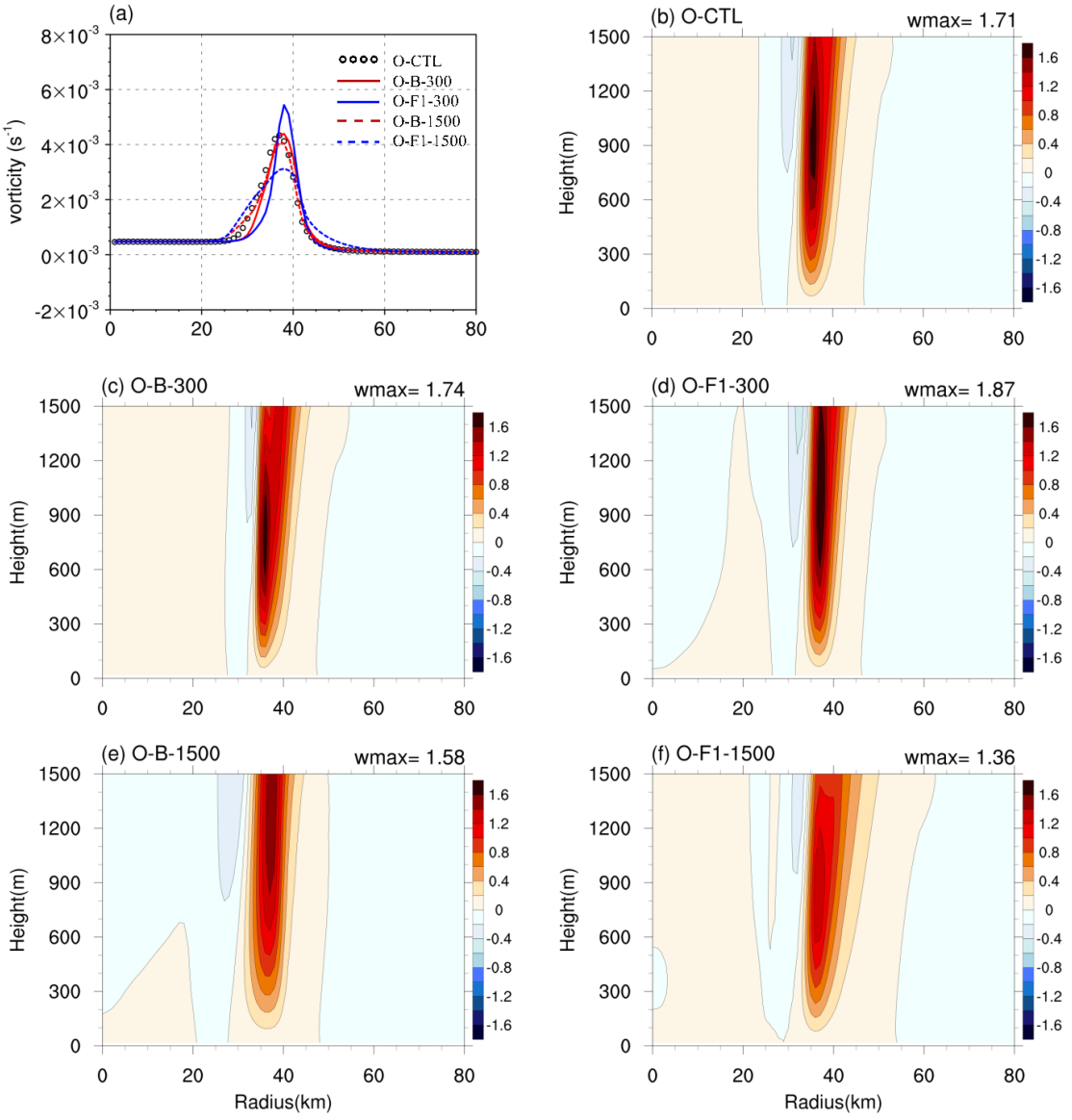

Figure 4. (a) Radial profiles of the absolute vertical vorticities in layer 1 of O-CTL (circles), O-B-300 (solid red), O-F1-300 (solid blue), O-B-1500 (dashed red), and O-F1-1500 (dashed blue) when v_{1m} increases from 30 to 35 m s^{-1}. Radius-height cross sections of vertical winds (unit: m s^{-1}) at the boundary layer top in (b) O-CTL, (c) O-B-300, (d) O-F1-300, (e) O-B-1500, and (f) O-F1-1500. Values on the top-right corners of panels (b)-(f) denote the updraft maximum.

The enhancement of radial flux of absolute vorticity in O-F1-300 is primarily due to the larger magnitude of absolute vorticity (Fig. 4a) related to the increased sharpness of the radial tangential wind profile near and inside the rmv_1 (Fig. 3c). On the contrary, with the horizontal mixing length enlarged in O-F1-1500, the radial flux of absolute vorticity decreases (Fig. 3e) due to the reduced sharpness of the radial tangential wind profile near and inside the rmv_1 (Fig. 4a), leading to the reduced net tendency of v_1 and thus smaller intensification rate. Furthermore, the modified feedback from the boundary layer because of changing l_h also plays a role in changing TC intensification (Figs. 4b-f). Enlarging l_h in the lower free atmosphere in C-F1-1500 effectively weakens the frictional updraft which controls the intensity of deep convection and the detrainment of air in the lower troposphere (Fig. 4f), thus reducing the inflow and inward flux of absolute vorticity and the intensification rate. In contrast, with l_h increased in the boundary layer (O-B-1500), frictional updraft is also reduced but the change is marginal (Fig. 4e). In addition, the upper-layer free atmosphere is almost a passive layer in response to the convective processes from below. As a result, changes in horizontal mixing length in the upper-layer free atmosphere has little effect on the overall intensity evolution of the simulated TC in OMBL.

4. Results from CM1 simulations

Although the OMBL model provides a convenient way to distinguish the respective effects of the lateral mixing in the boundary layer and in the free atmosphere, it includes many simplifications. Next, the results from OMBL simulations discussed in section 3 are further validated/confirmed with simulations using both the axisymmetric and three-dimensional versions of CM1 as described in section 2c.

a. Axisymmetric simulations

Figure 5 shows the evolution characteristics of the TC simulated in the axisymmetric version of CM1, including TC intensity in terms of maximum 10-m height tangential wind speed (v_{10m}) and central sea level pressure (p_{min}), intensification rate (24-h intensity change in v_{10m}), and the radius of v_{10m} in C-CTL, C-z1.5-1500, C-z.15-10-1500, C-lz10-1500, and C-ALL-1500. We can see distinct differences in TC intensity evolution among these experiments no matter in terms of v_{10m} or p_{min}. In terms of v_{10m}, increasing the horizontal mixing length from 700 m to 1500 m in the whole model domain (C-ALL-1500) reduces the quasi-steady TC intensity by 17.4% (Fig. 5a). This reduced intensity is predominantly

attributed to the larger horizontal diffusion in the middle atmosphere (C-z1.5-10-1500), which alone reduces the quasi-steady TC intensity by 11.5%. Increasing the horizontal mixing length from 700 m to 1500 m in the boundary layer (C-z1.5-1500) causes a smaller (8.7%) reduction in the quasi-steady intensity. The differences in the steady-state p_{min} are generally consistent with those in v_{10m}. However, we notice that p_{min} in C-z1.5-10-1500 is much closer to that in C-ALL-1500, and that in C-z1.5-1500 is much closer to that in C-CTL (Fig. 5b) compared with the difference in v_{10m}. This implies that the horizontal diffusion also affects the simulated TC structure to some extent and partly changes the wind-pressure relationship (Bryan 2012). The inner-core size during the quasi-steady stage is consistent with the TC intensity (Figs. 5a,b,d), namely, with a stronger TC corresponding to a smaller inner-core size (in terms of the RMW).

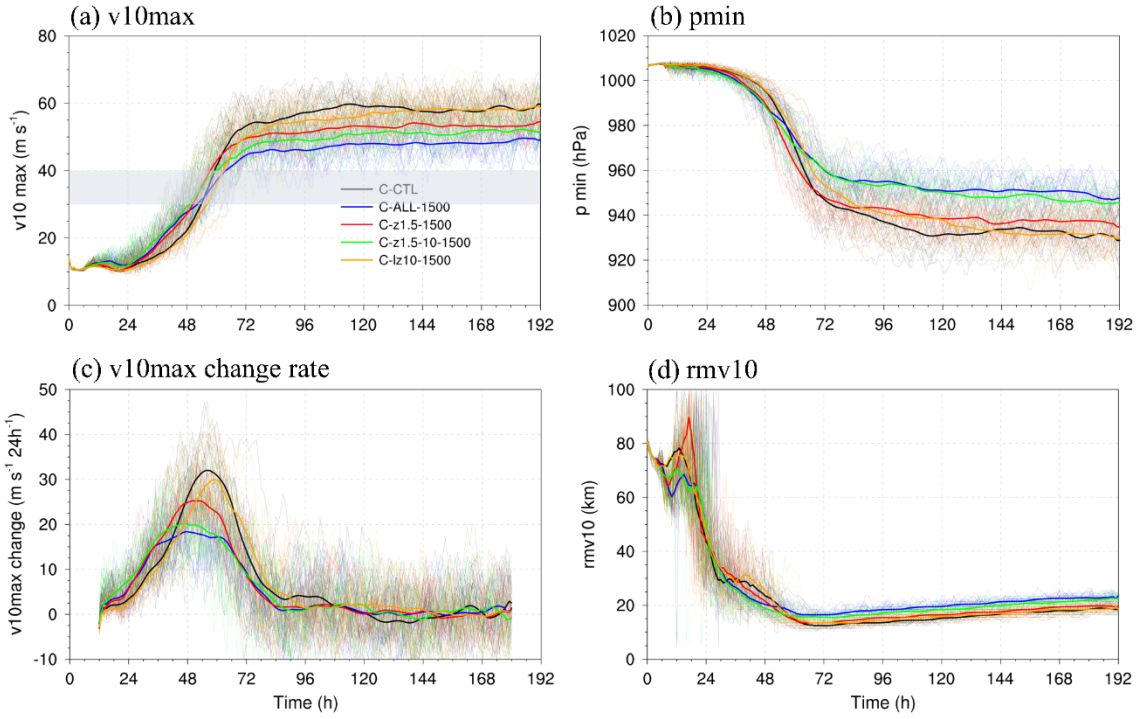

Figure 5. Time series of the ensemble-mean (a) maximum 10-m height tangential wind (v_{10m}), (b) minimum sea level pressure, (c) 24-h intensity change, and (d) the radius of v_{10m} in C-CTL (thick black), C-z1.5-1500 (thick red), C-z1.5-10-1500 (thick green), C-lz10-1500 (thick orange), and C-ALL-1500 (thick blue). Thin curves represent different ensemble members. The gray zone in (a) marks the period when the simulated TCs intensify from 30 to 40 m s^{-1}. Some further analyses about this intensifying period are conducted later and shown in Figs. 7-11 and 15.

The TC intensification rate (in terms of the 24-h intensity change) during the primary intensification stage is smaller in both C-ALL-1500 and C-z1.5-10-1500 than in C-CTL with the peak intensification rate reduced by 42.8% and 35.7%, respectively (Fig. 5c). In contrast,

the peak intensification rate in C-z1.5-1500 is only reduced by 20.6% compared to that in C-CTL. In addition, increasing horizontal mixing in the outflow layer (C-lz10-1500) has little effect on the TC intensification rate and maximum intensity. Different from that in the primary intensification stage, the spinup during the early intensification stage or the onset of the primary intensification does not slow down by enlarging the horizontal mixing length, but even is slightly accelerated. This is because the larger horizontal turbulent mixing favors the initial inward mixing of angular momentum (Fig. 7e) and the moistening in the inner core, and thus the earlier initiation of convective organization.

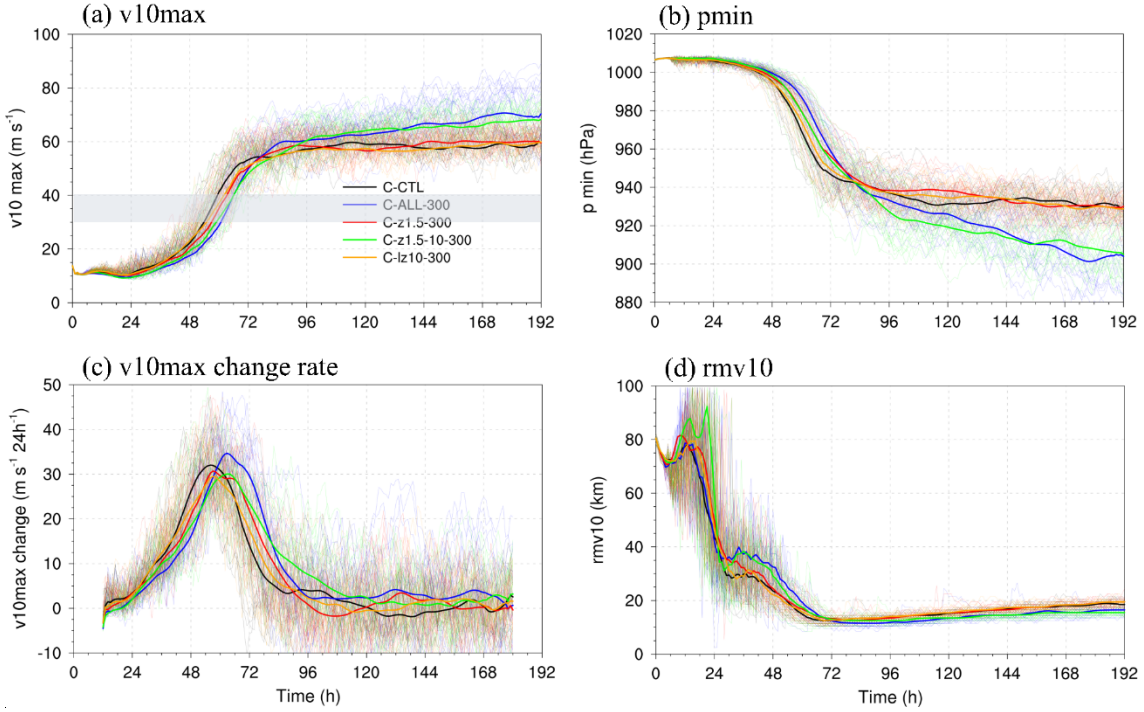

Figure 6. As in Fig. 5, but for C-CTL (thick black), C-z1.5-300 (thick red), C-z1.5-10-300 (thick green), C-lz10-300 (thick orange), and C-ALL-300 (thick blue).

Figure 6 shows the evolutions of variables as in Fig. 5 but for the set of experiments with the horizontal mixing length reduced. The most remarkable feature is that the quasi-steady intensities simulated in C-ALL-300 and C-z1.5-10-300 are larger than that simulated in C-CTL, with v_{10m} being 19.1% and 15.4% larger, respectively, while the intensity evolution simulated in C-z1.5-300 is similar to that in C-CTL (Figs. 6a,b). Although the differences in the intensification rate among these experiments with the reduced horizontal mixing length are not as obvious as those with the enlarged horizontal mixing length in Fig. 5, there are still some differences during the late primary intensification stage. The TCs simulated in C-ALL-300 and C-z1.5-10-300 show longer intensification periods than those in C-CTL and C-z1.5-300 during the late intensification stage. Overall, the results from the full-physics model

simulations demonstrate that the horizonal diffusion in the middle troposphere has a considerably larger impact on the simulated TC intensification rate and quasi-steady intensity than that in the boundary layer, while that in the outflow layer has little effect on both. This is consistent with the conclusion from the Ooyama-type model discussed in section 3 although some differences in details exist.

To understand how the horizontal diffusion affects the TC intensification in the axisymmetric CM1 simulations, we also performed a tangential wind budget analysis. The equation for the local tendency of tangential wind (v) in the axisymmetric CM1 is given as:

$$\frac{\partial v}{\partial t} = -u\zeta_a - w\frac{\partial v}{\partial z} + D_{vd,v} + D_{hd,v}, \quad (2)$$

where $\zeta_a = f + \frac{v}{r} + \frac{\partial v}{\partial r}$ is the absolute vertical vorticity. Terms on the right-hand side denote the tendency terms due to the radial flux of absolute vorticity (v-hadv), the vertical advection of tangential wind (v-vadv), and the vertical and horizontal diffusions of tangential wind (v-vturb, v-hturb), respectively. The formulae of $D_{vd,v}$ and $D_{hd,v}$ can be found in section 2a of BR09a. The net v tendency (v-net) and all tendency components during the primary intensification stage (from 30 to 40 m s^{-1} as marked in Fig. 5 by gray range) of the simulated TC in C-CTL are shown in Fig. 7. We can see that the net local v tendency peaks inside the RMW at all levels (Fig. 7a), facilitating the eyewall contraction and intensification of the simulated TC (Li et al. 2021). In general, the radial flux of absolute vorticity dominates the positive tangential wind tendency and TC intensification in the boundary layer (Fig. 7c). The vertical advection contributes to the positive tangential wind tendency near and inside the RMW above the boundary layer (Fig. 7b), where, however, the positive tendency is largely offset by the negative radial flux of absolute vorticity (Fig. 7c) associated with the shallow outflow induced by the outward agradient force due to the upward advection of supergradient wind component from the boundary layer (Li et al. 2020; Fei et al. 2021). Note that the positive tangential wind tendency contributed by the radial flux of absolute vorticity in the boundary layer (Fig. 7c) is largely counteracted by the negative tendency due to vertical diffusion including surface friction (Fig. 7d). The horizontal diffusion imposes a direct negative contribution to tangential wind tendency near the RMW with the maximum magnitude in the lower boundary layer (Fig. 7e), which is consistent with RB12 (p. 2296). However, the horizontal diffusion in the free atmosphere is found to have a more pronounced total effect on TC intensification and the steady-state intensity than that in the boundary layer (Figs. 5 and 6), as detailed further (see results given in Figs. 8–11).

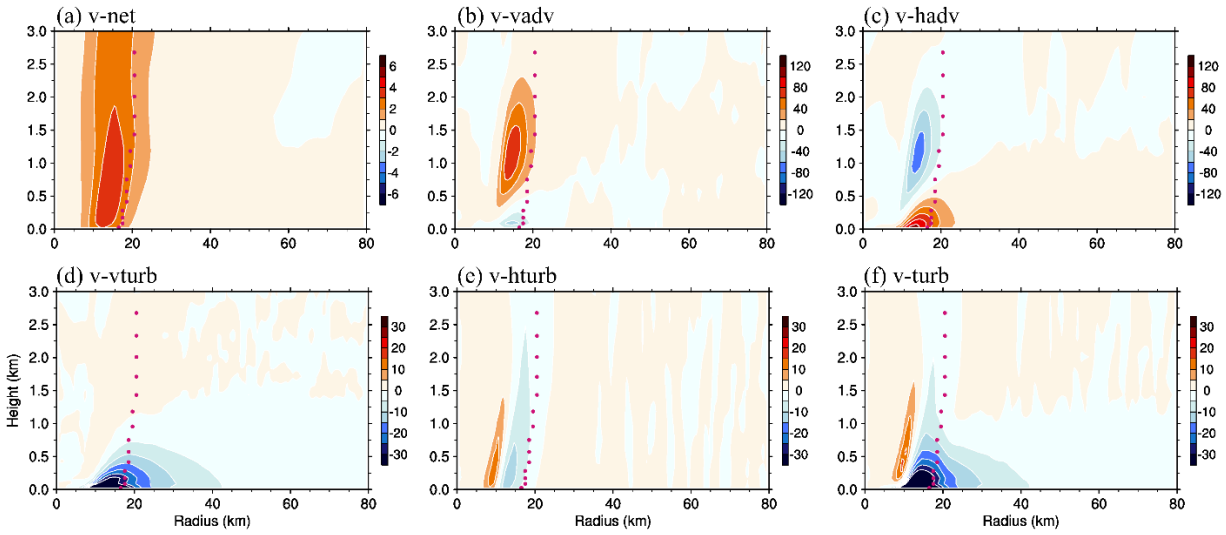

Figure 7. Radius-height distributions of the ensemble-mean tendency terms of tangential wind (unit: m s^{-1} h^{-1}) in C-CTL when the simulated TC intensifies from 30 to 40 m s^{-1}. The tendency terms include (a) the net tendency (v-net), (b) vertical advection (v-vadv), (c) radial flux of absolute vorticity (v-hadv), (d) vertical diffusion (v-vturb), (e) horizontal diffusion (v-hturb), and (f) total diffusion [(v-turb) = (v-hturb) + (v-vturb)]. Deep pink dots denote the RMW, which are also shown in Figs. 8-11,13,15. Note that the color bars of different panels are different.

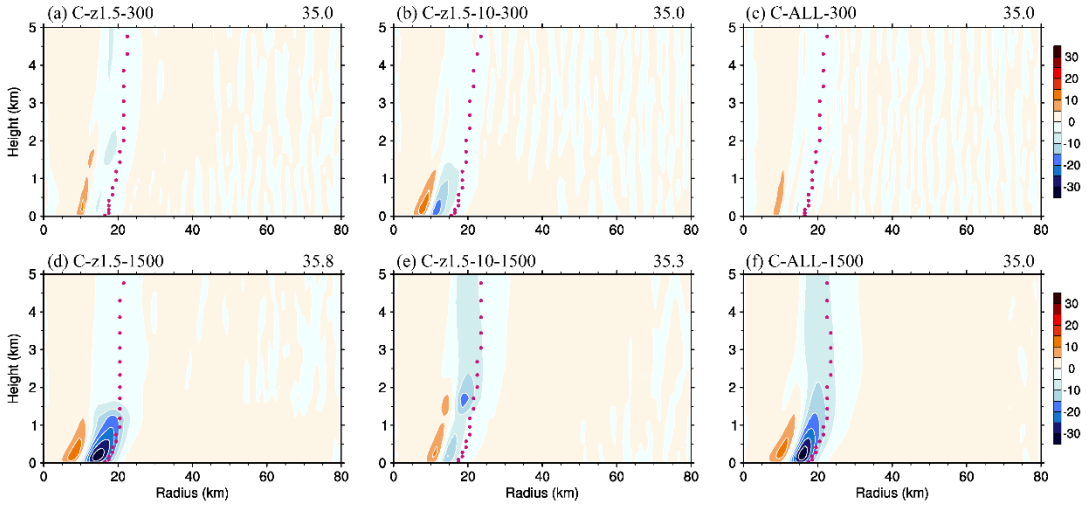

Figure 8. Radius-height diagrams of the ensemble-mean horizontal diffusion of tangential wind (unit: m s^{-1} h^{-1}) in (a) C-z1.5-300, (b) C-z1.5-10-300, (c) C-ALL-300, (d) C-z1.5-1500, (e) C-z1.5-10-1500, and (f) C-ALL-1500 when the simulated TCs intensify from 30 to 40 m s^{-1}. The values at the top-right corners are the average TC intensities (unit: m s^{-1}) in terms of maximum 10-m height tangential wind during the chosen intensifying period.

Figure 8 compares the tangential wind tendencies due to horizontal diffusion in all axisymmetric CM1 simulations, averaged in the periods when the simulated TCs intensified from 30 to 40 m s^{-1} (marked in Figs. 5 and 6), during which the time-averaged intensities are similar among all simulations (as labelled in each panel). Note that since the corresponding

changes in simulations with l_h modified in the outflow layer (C-lz10-300 and C-lz10-1500) show very marginal, the results are not shown. Reducing (enlarging) the horizontal mixing length in the boundary layer and/or the free atmosphere leads to a marked decrease (increase) in the absolute magnitude of the horizontal diffusion of tangential wind in the inner core of the corresponding region. However, changing l_h above the boundary layer also slightly modifies the horizontal tangential wind diffusion in the boundary layer in addition to its direct influence on the tangential wind diffusion above the boundary layer. This implies that the horizontal mixing above the boundary layer has some effect on the boundary layer wind structure. This is mainly because the boundary layer flow is largely controlled by the interior flow above.

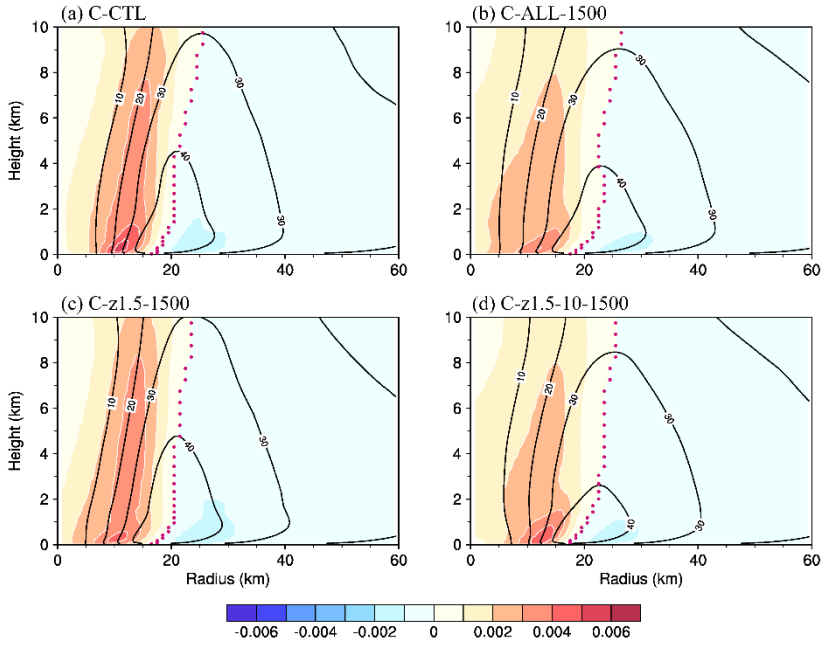

Figure 9. Radius-height diagrams of the ensemble-mean tangential wind (contour; unit: m s^{-1}) and its radial gradient (shaded; unit: s^{-1}) in (a) C-CTL, (b) C-ALL-1500, (c) C-z1.5-1500, and (d) C-z1.5-10-1500 when the simulated TCs intensify from 30 to 40 m s^{-1}.

The horizontal diffusion acts to reduce the sharpness of the tangential wind profile inside the RMW as indicated in section 3. This can be seen from Fig. 9, which shows the radius-height cross sections of tangential wind and its radial gradient ($\partial v/\partial r$), both averaged in the chosen periods as marked in Fig. 5a for simulations with l_h enlarged from 700 m to 1500 m. The results in those experiments with the horizontal mixing length reduced from 700 m to 300 m are generally consistent and are not shown. Comparing Figs. 9a and 9b, we can see that larger radial diffusion in the whole model atmosphere considerably reduces the radial gradient of tangential wind inside the RMW throughout the troposphere, and accordingly the

radial profile of tangential wind becomes less peaked near the RMW. Enlarging the horizontal mixing length below 1.5-km height in the boundary layer (C-z1.5-1500) only leads to the reduced radial gradient of tangential wind inside the RMW in a very shallow layer near the surface (Fig. 9c). In contrast, the radial gradient of tangential wind in C-z1.5-10-1500 is reduced inside the RMW, no matter above or within the boundary layer (Fig. 9d). This indicates that the horizontal diffusion in the free troposphere has a more significant effect on the simulated TC structure and thus the intensity evolution than that in the boundary layer.

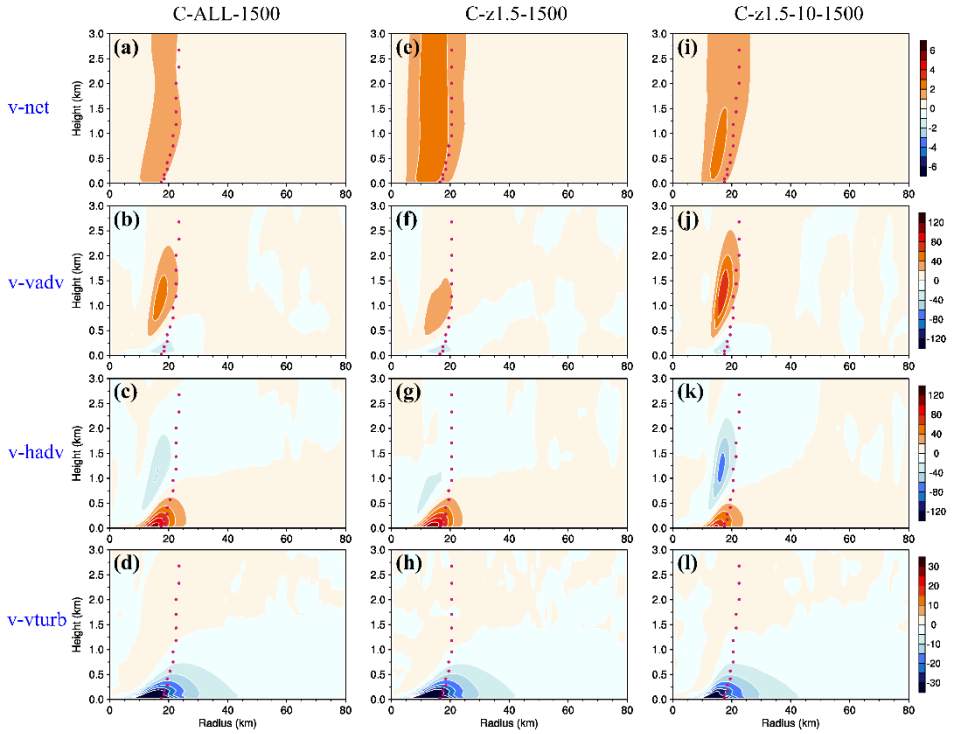

Figure 10. Radius-height diagrams of the ensemble-mean tendency terms of tangential wind (unit: m s^{-1} h^{-1}) in (a-d) C-ALL-1500, (e-h) C-z1.5-1500, and (i-l) C-z1.5-10-1500. The tendency terms include (top row) the net tendency, (second row) vertical advection, (third row) radial flux of absolute vorticity, and (bottom row) vertical diffusion. Note that horizontal diffusion has been given in Figs. 8d-f.

Tangential wind tendencies of sensitivity experiments are shown in Fig. 10 for a better comparison with that of C-CTL given in Fig. 7. The net tangential wind tendencies in C-ALL-1500 and C-z1.5-10-1500 are substantially reduced compared to that in C-CTL (Figs. 10a,i), which is consistent with the smaller intensification rates in the former two experiments (Fig. 5). The net tangential wind tendency in C-z1.5-1500 is also reduced but not as obviously as those in the other two sensitivity experiments. It is the decrease in the inward flux of absolute vorticity (Fig. 10k) that accounts for the decrease in the net tangential wind tendency in C-z1.5-10-1500 (Fig. 10i). The weaker inward flux of absolute vorticity in C-z1.5-10-1500 is a result of the smaller absolute vorticity in the boundary layer due to changes

in the TC wind structure (Fig. 9d). On the contrary, an increase in the inward flux of absolute vorticity occurs in C-z1.5-1500 (Fig. 10g), which partly offsets the increase in the negative tangential wind tendency induced by the enhanced horizontal diffusion in the boundary layer. As a result, both the intensification rate and steady-state intensity are somewhat reduced. The stronger inward flux of absolute vorticity in C-z1.5-1500 is due to the stronger inward horizontal mixing of radial wind in the boundary layer, which makes the inflow to penetrate more inward from the inflow core and maintain a certain strength inside the RMW where the absolute vorticity is large (Fig. 11). Nevertheless, overall, the results from the axisymmetric full-physics model CM1 support the main conclusions drawn from the simple Ooyama-type model. Namely, the horizontal diffusion in the middle-lower troposphere has a more pronounced effect on the intensification rate and the steady-state intensity of the simulated TC than that in the boundary layer while that in the outflow layer has little effect on both.

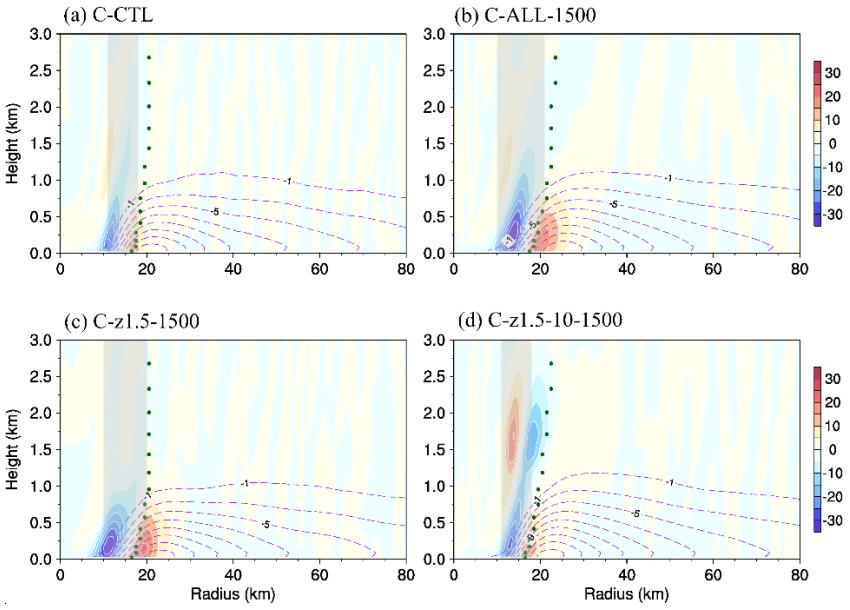

Figure 11. Radius-height diagrams of the ensemble-mean radial wind (contoured at an interval of -2 m s^{-1} from -1 m s^{-1}) and its tendency due to horizontal diffusion (shaded; unit: m s^{-1} h^{-1}) in (a) C-CTL, (b) C-ALL-1500, (c) C-z1.5-1500, and (d) C-z1.5-10-1500. The gray zone in each panel denotes the radial range where the inflow on the lowest model level weakens from 15 to 2 m s^{-1}.

b. Three-dimensional simulation

Figure 12 shows time series of the maximum azimuthally averaged 10-m height tangential wind speed and its 24-h change in the three-dimensional simulations with CM1. Compared with the results of axisymmetric (Figs. 5 and 6) and three-dimensional simulations (Fig. 12), the changes in TC intensification rates and mature intensities caused by modifying l_h in different vertical regions are generally similar. This demonstrates that the finding that

the horizontal diffusion above the boundary layer has a more pronounced impact on TC intensity is tenable no matter the asymmetric eddies are included or not.

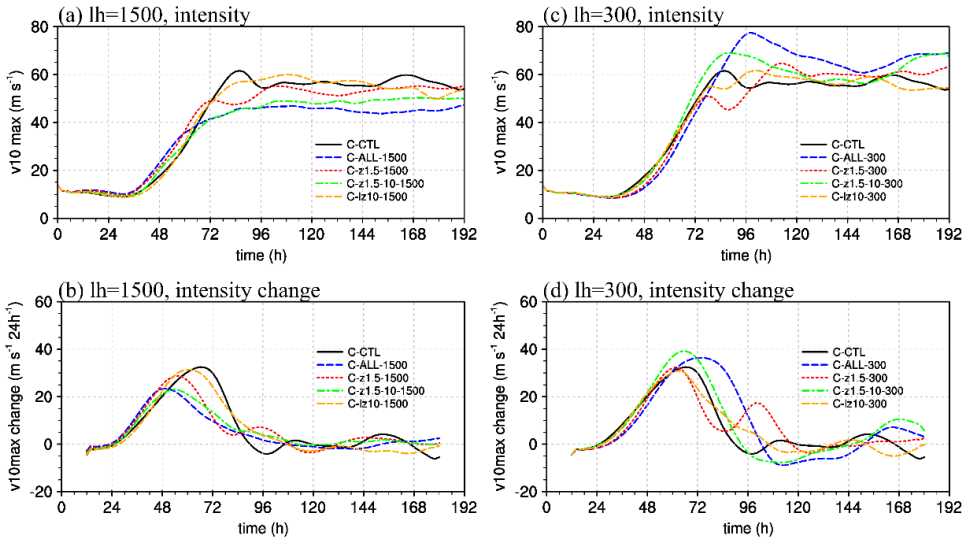

Figure 12. Time series of (a) maximum azimuthally averaged 10-m height tangential wind (v_{10m}) and (b) 24-h intensity change in the three-dimensional version of C-CTL (black), C-z1.5-1500 (red), C-z1.5-10-1500 (green), C-lz10-1500 (orange), and C-ALL-1500 (blue). Panels (c) and (d) are similar to (a) and (b) respectively but for the sensitivity experiments with l_h shortened to 300 m.

The azimuthally-averaged tangential wind budget analysis is performed for the three-dimensional simulations to further elucidate the dynamical mechanisms, in particular the effects of asymmetric eddy motion. Following Xu and Wang (2010), the budget equation of the azimuthally average tangential wind is given by

$$\frac{\partial \bar{v}}{\partial t} = -\bar{u}\bar{\zeta}_a - \bar{w}\frac{\partial \bar{v}}{\partial z} - u'\zeta_a{}' - \overline{w'\frac{\partial v'}{\partial z}} + \overline{D_{vd,v}} + \overline{D_{hd,v}}, \qquad (3)$$

where variables or terms with an overbar denote the azimuthal average, and those with a prime represent the deviations from the corresponding azimuthal average (namely the asymmetric eddy). The terms on the right-hand side of Eq. (3) are, respectively, the mean radial flux of absolute vertical vorticity, the mean vertical advection of the azimuthally mean tangential wind, the radial eddy flux of eddy vorticity, the vertical advection of eddy tangential wind, parameterized vertical diffusion, and parameterized horizontal diffusion. To investigate the role of horizontal mixing in different vertical regions, the net wind tendency (v-net), the total azimuthal mean contribution (v-adv, the first two terms on the right-hand side of Eq. 3), the sum of the eddy terms (v-eddy, the third and fourth terms), and the sum of diffusion terms (v-turb, the last two terms) are calculated and compared among different experiments. Note that the results of the experiments with l_h of 300 m are consistent with

those of 1500 m, and thus only the results of the experiments with l_h enlarged to 1500 m are discussed below. Figure 13 shows 3-h average of the terms in the azimuthally averaged tangential wind budget equation Eq. (3) when the TC intensities are about 30 m s^{-1} (during the period of rapid intensification) in the three-dimensional experiments C-CTL, C-ALL-1500, C-z1.5-1500, and C-z1.5-10-1500. Compared to that in C-CTL, the net tendencies of $\bar{v}$ are reduced to different extents in C-ALL-1500, C-z1.5-1500, and C-z1.5-10-1500 (Figs. 13a-d), which is consistent with the reduced TC intensification rates shown in Fig. 12b.

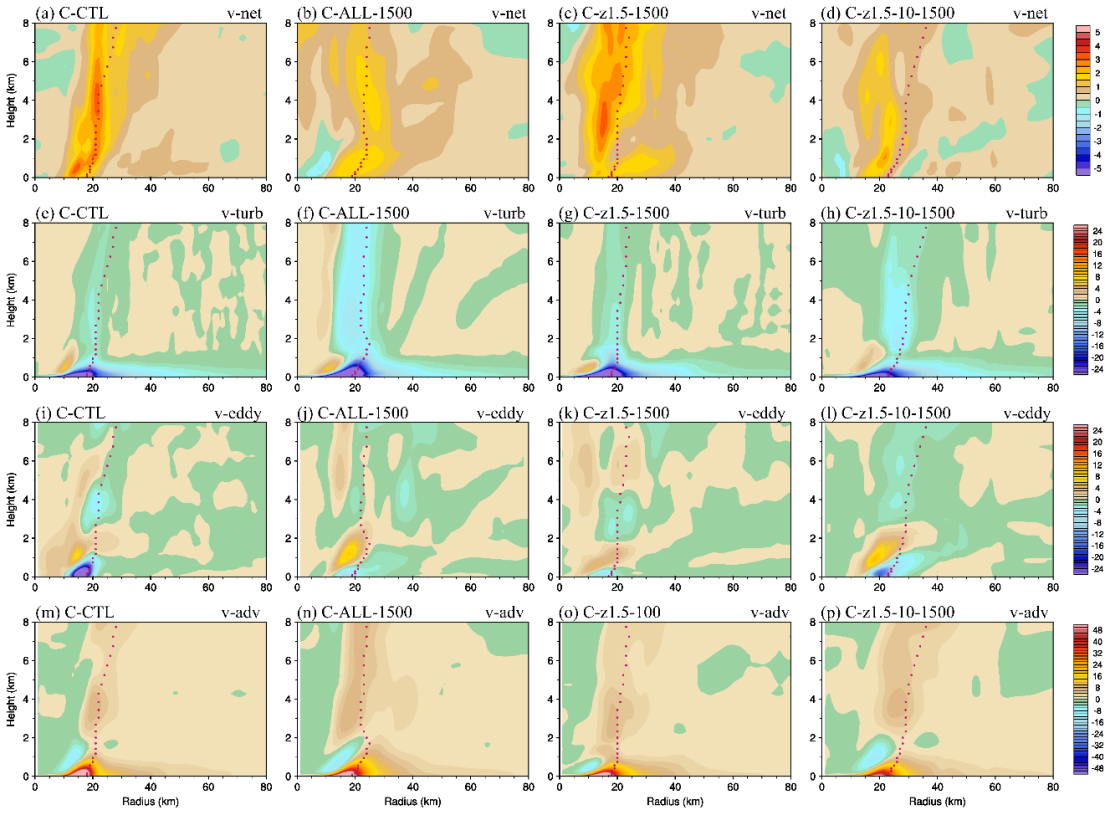

Figure 13. Radius-height distributions of the tendency terms of azimuthally averaged tangential winds (unit: m s^{-1} h^{-1}) in C-CTL (leftmost column), C-ALL-1500 (second column from the left), C-z1.5-1500 (third column from the left), and C-z1.5-10-1500 (rightmost column) when the simulated TC intensities are around 30 m s^{-1}. The tendency terms include the net tendency (v-net; top row), parameterized diffusion (v-turb=$\overline{D_{vd,v}} + \overline{D_{hd,v}}$; second row), the sum of the eddy transport (v-eddy=$-\overline{u'\zeta_a{}'} - \overline{w'\frac{\partial v'}{\partial z}}$; third row), and the total mean advection (v-adv=$-\bar{u}\bar{\zeta}_a - \bar{w}\frac{\partial \bar{v}}{\partial z}$; bottom row). Deep pink dots denote the RMW. Note that the color bars on different rows are different.

In all simulations, the total mean advection (Figs. 13m-p) and the diffusion term (Figs. 13e-h) are the main contributors to the positive and negative tendency of $\bar{v}$, respectively, especially in the boundary layer. In the control experiment, the eddy term is also a significant negative contributor to $\bar{v}$ tendency around the eyewall and is comparable to the parameterized

551 diffusion term in the boundary layer (Fig. 13i). Previous studies of three-dimensional
552 numerical simulations of TC also found that resolved eddies tended to spin down the
553 tangential wind speed in the boundary layer of TC eyewall (Wang 2002; Wu and Braun 2004;
554 Zhang and Marks 2015). After enlarging l_h throughout the model domain (C-ALL-1500), the
555 eddy contribution to the negative $\bar{v}$ tendency in the boundary layer is much smaller. Similar
556 phenomenon was also found by Zhang and Marks (2015) through a budget analysis of
557 absolute angular momentum using the output from a three-dimensional Hurricane Weather
558 and Research Forecasting model simulation (cf. their Fig. 9). The weakened eddy
559 contribution is related to the suppressed eddy activities by the strong horizontal diffusion in
560 C-ALL-1500. This can be seen clearly from Fig. 14, which exhibits the time evolutions of
561 eddy kinetic energy [$=(u'^2 + v'^2)/2$] averaged within 1.2 times of the RMW in the three-
562 dimensional CM1 simulations. Enlarging l_h throughout the model domain results in a
563 substantial reduction of the eddy kinetic energy, which agrees with the finding by Zhang and
564 Marks (2015) who found that larger l_h corresponded to smoother horizontal distributions of
565 vertical wind and relative vorticity (cf. their Fig. 10).

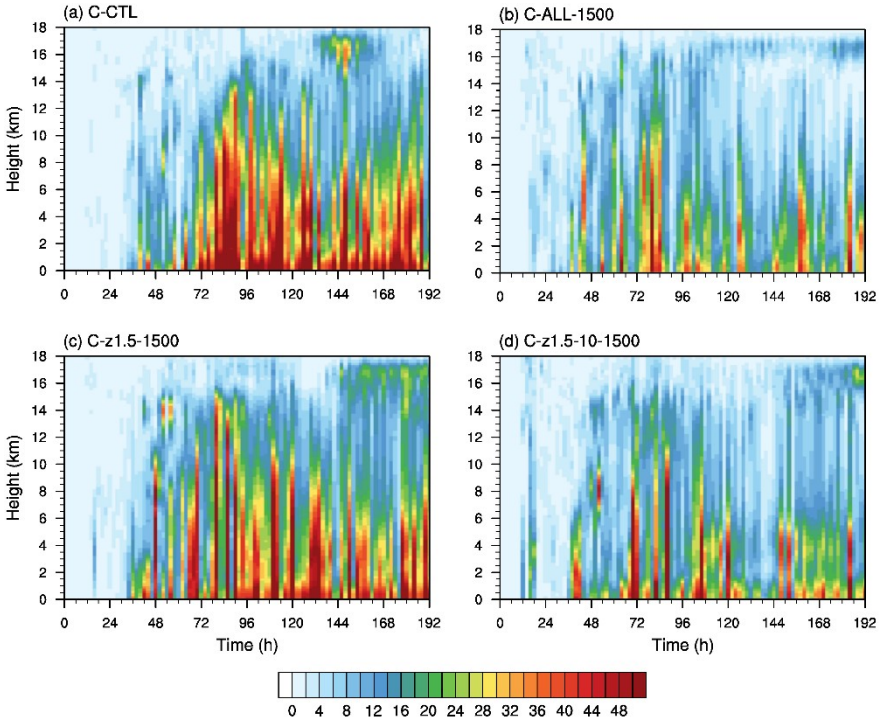

566

567 Figure 14. Time-height diagrams of the eddy kinetic energy (unit: $m^2 s^{-2}$) which is averaged within 1.2
568 times of RMW in the three-dimensional version of (a) C-CTL, (b) C-ALL-1500, (c) C-z1.5-1500, and (d)
569 C-z1.5-10-1500.

570 In the simulation with l_h only increased in the boundary layer (C-z1.5-1500), the
571 magnitude of negative diffusion term is strengthened in the boundary layer (Fig. 13g).

572 Accordingly, the eddy activity in the shallow layer is restrained (Fig. 14c) and the negative
573 contribution from the eddy term to the $\bar{v}$ tendency near the eyewall is reduced (Fig. 13k).
574 With the horizontal mixing enlarged above the boundary layer, the positive azimuthal mean
575 contribution to the $\bar{v}$ tendency is reduced in the boundary layer (Fig. 13p). Note that changes
576 in the azimuthally averaged tangential wind structure are consistent with those in
577 axisymmetric simulations discussed earlier in section 4a (Figs. 9d and 10k) and thus are not
578 shown. Besides modulating the azimuthal mean contribution, the horizontal mixing above the
579 boundary layer also shows an effect on the boundary-layer eddy activity. The eddy kinematic
580 energies both above and within the boundary layer are reduced with the horizontal mixing
581 length enlarged above the boundary layer (Fig. 14d). Because of the suppressed resolved
582 eddies in the boundary layer, the negative contribution from the eddy term to the $\bar{v}$ tendency
583 is reduced accordingly to some extent (Fig. 13l), though it is not so pronounced as that in C-
584 z1.5-1500 (Fig. 13k). This further indicates that consistent with the axisymmetric CM1
585 simulations, changing the parameterized horizontal diffusion above the boundary layer
586 affects the boundary-layer wind structure and the intensity of the simulated TC. Such effects
587 include the effect on the azimuthal mean TC structure and the effect on the eddy activities. In
588 three-dimensional experiments, the negative effect of the parameterized horizontal diffusion
589 on TC intensification is less remarkable than that in axisymmetric experiments because
590 mainly because the eddy activity has a negative effect on tangential wind budget near the
591 RMW, which is also reduced by the enhanced parameterized horizontal diffusion.

592 ## 5. Conclusions and discussion

593 Previous numerical studies have shown that horizontal diffusion can impose significant
594 impacts on TC intensification and maximum intensity and attributed such impacts to the
595 horizonal diffusion in the boundary layer. Enhanced horizontal diffusion can reduce the radial
596 gradient of absolute angular momentum and thus the inward transport of absolute angular
597 momentum from the outer core region, leading to the reduced intensification rate and
598 maximum intensity. However, most previous studies have examined the sensitivity of the
599 simulated TC intensity evolution to the horizontal diffusion by varying the horizontal mixing
600 length throughout the model atmosphere (BR09a; Bryan 2012; RB12; Zhang and Marks
601 2015). It is unclear the relative importance of horizontal diffusions in the boundary layer and
602 in the free atmosphere. To address this issue, we performed sensitivity numerical experiments
603 by varying the horizontal mixing length in the boundary layer and in the free atmosphere

either together or separately in the axisymmetric Ooyama-type three-layer model with a multilevel boundary (OMBL, FW21) and the axisymmetric and three-dimensional versions of the full-physics cloud model CM1 (BR09a).

Results from the OMBL model show that enlarging (reducing) the horizontal mixing length in the lower-layer free atmosphere considerably reduces (increases) the intensification rate and the steady-state intensity of the simulated TC, while changing the horizontal mixing length in the boundary layer or in the upper-layer free atmosphere has little effect. The tangential wind budget analysis indicates that in addition to the direct negative contribution to the tangential wind tendency, the horizontal diffusion in the lower-layer free atmosphere also leads to a decrease in the tangential wind tendency near and immediately inside the RMW by reducing the inward flux of absolute vorticity. Since in the OMBL model the boundary layer flow is largely driven by the flow (and pressure gradient force) above the boundary layer, changing the horizontal mixing length in the boundary layer has little effect on the tangential wind budget above the boundary layer. In addition, because the upper-layer free atmosphere is almost a passive layer in response to the convective processes from below, changes in horizontal mixing length in the upper-layer free atmosphere almost has no effect on the overall intensity evolution of the simulated TC.

The basic results of CM1 experiments, no matter with the axisymmetric or three-dimensional versions, are generally consistent with those of OMBL. Namely, the horizontal mixing in the middle-lower troposphere (the layer between 1.5 and 10 km heights) has a pronounced effect on TC intensification rate and maximum intensity, and that in the outflow upper troposphere (above 10 km) has little effect. Tangential wind budget analysis indicates that the horizontal diffusion in the middle-lower troposphere reduces the tangential wind tendency by reducing the inward flux of absolute vertical vorticity in the boundary layer, which is because the boundary-layer wind structure is largely controlled by the interior flow above. This finding supports the conjecture proposed by RB12 who suggested that horizontal diffusion may influence TC intensity through adjusting interior flow. Modifying the horizontal mixing length in the boundary layer (below 1.5 km) in CM1 experiments also causes a nonnegligible change in TC intensity, although the change is not as large as that induced by modifying the mixing in the middle-lower troposphere. This is because the horizontal diffusion of tangential wind in the boundary layer has a direct negative effect on TC spinup. However, stronger horizontal diffusion of radial wind flattens the radial distribution of boundary-layer inflow, making the inflow penetrates more inward from the

637 inflow core and thus increasing the radial flux of absolute vorticity near the RMW. The latter
638 partly offsets the direct negative contribution from the horizontal diffusion of tangential wind
639 but still results in a nonnegligible decrease in the intensification rate and the steady-state
640 intensity of the simulated TC. In the three-dimensional CM1 simulations, the horizontal
641 mixing also affects the activities of resolved asymmetric eddies. Results from the azimuthal
642 mean tangential wind budget analysis show that the resolved eddies contribute negatively to
643 the azimuthal mean tangential wind tendency near the RMW, especially in the boundary
644 layer. This negative effect is often relatively large when a small horizontal mixing length is
645 used but is considerably suppressed when the horizontal mixing length is large. This is
646 because large horizontal mixing length both within and above the boundary layer suppresses
647 eddy activities.
648 Note that although the results from the full-physics model CM1 support the major finding
649 based on the simple OMBL model, changing the horizontal mixing in the boundary layer in
650 the CM1 simulations shows some visible effect on TC intensity, which is different from that
651 in the OMBL simulations. This is mainly due to the different model frameworks of the two
652 models. In OMBL, the TC intensity refers to the maximum tangential wind in the lower free
653 atmosphere layer in our analysis, which is characterized by the interior flow and is more
654 easily affected by the horizontal diffusion in this layer. However, in CM1, the maximum 10-
655 m height tangential wind is deemed as TC intensity, which is partly affected by the inherent
656 boundary-layer processes although the latter is largely controlled by the interior flow.
657 In addition, we found that the effect of horizontal diffusion is not obvious until the
658 simulated TC reaches a certain intensity. This is because the absolute value of horizontal
659 diffusion is relatively small compared to other tangential wind tendency terms in the early
660 intensification stage. The absolute value increases as the TC intensifies, and thus giving rise
661 to increasing impacts on the intensification rate in the late intensification stage and the
662 steady-state intensity of the simulated TC.
663 Finally, we should point out that the dynamics and thermodynamics are coupled in CM1
664 and in nature. Change in the horizontal mixing length affects not only momentum but also
665 thermodynamic variables. BR09a mentioned that the weaker radial gradient of potential
666 temperature resulting from horizontal diffusion above the boundary layer indicates smaller
667 vertical shear of tangential wind in the eyewall due to approximate thermal wind balance.
668 Figure 15 shows the radial gradient of the potential temperature in CM1 sensitivity
669 experiments. Enlarging the horizontal mixing in the free troposphere or throughout the whole

model domain reduces the radial gradient of potential temperature to some degree, while modifying the horizontal mixing length in the boundary layer induces little change. This seems to suggest that horizontal diffusion in the free troposphere imposes more effect on both the dynamic and thermodynamic structures of the simulated TC. Nevertheless, the major difference in the radial gradient of potential temperature between C-ALL-1500 (or C-z1.5-10-1500) and C-CTL is apparent only in the eye region and not across the eyewall. This is consistent with the statement of BR09a who indicated that TC intensity is more sensitive to horizontal diffusion of momentum than to that of scalars. Our results thus seem to support the notion that the dynamical effect of horizontal diffusion is predominant in affecting the simulated TC evolution in comparison to the thermodynamical effect.

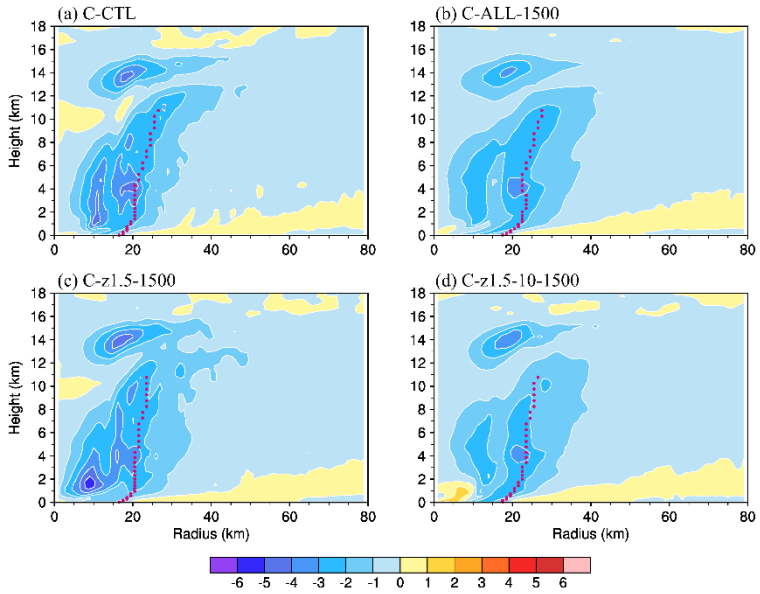

Figure 15. Radius-height diagrams of the ensemble-mean radial gradient of potential temperature (K m^{-1}) in the axisymmetric CM1 simulations of (a) C-CTL, (b) C-ALL-1500, (c) C-z1.5-1500, and (d) C-z1.5-10-1500 when the simulated TCs intensify from 30 to 40 m s^{-1} during the primary intensification stage.

This study offers new insights to understanding how horizontal diffusion influences the intensification and the maximum intensity of numerically simulated TCs. Results from this study also recall the view that the interior flow predominantly controls the boundary-layer flow, while the latter feeds back to the interior flow through its control on the radial location and strength of eyewall updraft. It is this coupled/interactive processes that determine the TC intensification and maximum intensity, and the sensitivity of the simulated TC intensity evolution to the initial TC vortex structure, as recently elaborated by Li and Wang (2021a,b). Future studies should devote more efforts to examining how the dynamical and

693 thermodynamical processes affect the interior flow and how the interior flow structure
694 influences TC intensification and maximum intensity. To address these issues may help better
695 understand the intensification processes and the prediction of TC intensity.

696 *Acknowledgments.*

697 The authors are grateful to three anonymous reviewers for their constructure review
698 comments, which helped improve the work and the manuscript. This study was supported in
699 part by the National Key R&D Program of China under grant 2017YFC1501602 and in part
700 by the National Natural Science Foundation of China under grant 41730960 and the NSF
701 grant AGS-1834300.

702 *Data Availability Statement.*

703 The numerical model simulations upon which this study is based are too large to archive
704 or to transfer. Instead, we provide the information needed to replicate the simulations; we
705 used CM1 model version [V19.10]. The model code, compilation script and other relevant
706 documentations are available at [https://www2.mmm.ucar.edu/people/bryan/cm1/].

707 REFERENCES

708 Braun, S. A., and W-K. Tao, 2000: Sensitivity of high-resolution simulations of Hurricane
709 Bob (1991) to planetary boundary layer parameterizations. *Mon. Wea. Rev.*, **128**, 3941–
710 3961, https://doi.org/10.1175/1520-0493(2000)129<3941:SOHRSO>2.0.CO;2.
711 Bryan, G. H., 2012: Effects of surface exchange coefficients and turbulence length scales on
712 the intensity and structure of numerically simulated hurricanes. *Mon. Wea. Rev*, **140**,
713 1125–1143, https://doi.org/10.1175/MWR-D-11-00231.1.
714 Bryan, G. H., and R. Rotunno, 2009a: The maximum intensity of tropical cyclones in
715 axisymmetric numerical simulations. *Mon. Wea. Rev*, **137**, 1770–1789,
716 https://doi.org/10.1175/2008MWR2709.1.
717 Bryan, G. H., and R. Rotunno, 2009b: Evaluation of an analytical model for the maximum
718 intensity of tropical cyclones. *J. Atmos. Sci*, **66**, 3042–3060,
719 https://doi.org/10.1175/2009JAS3038.1.
720 Drennan, W. M., J. A. Zhang, J. R. French, C. McCormick, and P. G. Black, 2007: Turbulent
721 fluxes in the hurricane boundary layer. Part I: Latent heat flux. *J. Atmos. Sci.*, **64**, 1103–
722 1115, https://doi.org/10.1175/JAS3889.1.
723 Donelan, M. A., B. K. Haus, N. Reul, W. J. Plant, M. Stiassnie, H. C. Graber, O. B. Brown,

and E. S. Saltzman, 2004: On the limiting aerodynamic roughness of the ocean in very strong winds. *Geophys. Res. Lett.*, **31**, L18306, https://doi.org/10.1029/2004GL019460.

Dunion, J. P., 2011: Rewriting the climatology of the tropical North Atlantic and Caribbean Sea atmosphere. *J. Climate*, **24**, 893–908, https://doi.org/10.1175/2010JCLI3496.1.

Eliassen, A., 1971: On the Ekman layer in a circular vortex. *J. Meteor. Soc. Japan*, **49**, 784–789.

Eliassen, A., and M. Lystad, 1977: The Ekman layer of a circular vortex: A numerical and theoretical study. *Geophys. Norv.*, **31**, 1-16.

Emanuel, K. A., 1986: An air–sea interaction theory of tropical cyclones. Part I: Steady-state maintenance. *J. Atmos. Sci.*, **43**, 585–604, https://doi.org/10.1175/1520-0469(1986)043<0585:AASITF>2.0.CO;2.

Emanuel, K. A., 1995: Sensitivity of tropical cyclones to surface exchange coefficients and a revised steady-state model incorporating eye dynamics. *J. Atmos. Sci.*, **52**, 3969–3976, https://doi.org/10.1175/1520-0469(1995)052<3969:SOTCTS>2.0.CO;2.

Emanuel, K. A., 1997: Some aspects of hurricane inner-core dynamics and energetics. *J. Atmos. Sci.*, **54**, 1014–1026, https://doi.org/10.1175/1520-0469(1997)054<1014:SAOHIC>2.0.CO;2.

Fei, R., Y. Wang, and Y. Li, 2021: Contributions of vertical advection to supergradient wind in tropical cyclone boundary layer: A numerical study. *J. Atmos. Sci.*, **78**, 1057–1073, https://doi.org/10.1175/JAS-D-20-0075.1.

Fei, R., and Y. Wang, 2021: Tropical cyclone intensification simulated in the Ooyama-type three-layer model with a multilevel boundary layer. *J. Atmos. Sci.*, **78**, 3799–3813, https://doi.org/10.1175/JAS-D-21-0127.1.

Gopalakrishnan, S. G., F. Marks, J. A. Zhang, X. Zhang, J.-W. Bao, and V. Tallapragada, 2013: A study of the impacts of vertical diffusion on the structure and intensity of the tropical cyclones using the high-resolution HWRF system. *J. Atmos. Sci.*, **70**, 524–541, https://doi.org/10.1175/JAS-D-11-0340.1.

Kepert, J., 2001: The dynamics of boundary layer jets within the tropical cyclone core. Part I: Linear theory. *J. Atmos. Sci.*, **58**, 2469–2484, https://doi.org/10.1175/1520-0469(2001)058<2469:TDOBLJ>2.0.CO;2.

Kepert, J., and Y. Wang, 2001: The dynamics of boundary layer jets within the tropical cyclone core. Part II: Nonlinear enhancement. *J. Atmos. Sci.*, **58**, 2485–2501, https://doi.org/10.1175/1520-0469(2001)058<2485:TDOBLJ>2.0.CO;2.

Li, T.-H., and Y. Wang, 2021a: The role of boundary layer dynamics in tropical cyclone intensification. Part I: Sensitivity to surface drag coefficient. *J. Meteor. Soc. Japan*, **99**, 537–554, https://doi.org/10.2151/jmsj.2021-027.

Li, T.-H., and Y. Wang, 2021b: The role of boundary layer dynamics in tropical cyclone intensification. Part II: Sensitivity to initial vortex structure. *J. Meteor. Soc. Japan*, **99**, 555–573, https://doi.org/10.2151/jmsj.2021-028.

Li, Y.-L., Y. Wang, and Y.-L. Lin, 2019: Revisiting the dynamics of eyewall contraction of tropical cyclones. *J. Atmos. Sci.*, **76**, 3229–3245, https://doi.org/10.1175/JAS-D-19-0076.1.

Li, Y.-L., Y. Wang, and Y.-L. Lin, 2020: How much does the upward advection of supergradient component of boundary-layer wind contribute to tropical cyclone intensification and maximum intensity? *J. Atmos. Sci.*, **77**, 2649–2664, https://doi.org/10.1175/JAS-D-19-0350.1.

Li, Y.-L., Y. Wang, Y.-L. Lin, and X. Wang, 2021: Why does rapid contraction of the radius of maximum wind precede rapid intensification in tropical cyclones? *J. Atmos. Sci.*, **78**, 3441-3453, https://doi.org/10.1075/JAS-D-21-0129.1.

Nolan, D. S., J. A. Zhang, and D. P. Stern, 2009a: Evaluation of planetary boundary layer parameterizations in tropical cyclones by comparison of in situ observations and high-resolution simulations of Hurricane Isabel (2003). Part I: Initialization, maximum winds, and the outer-core boundary layer. *Mon. Wea. Rev.*, **137**, 3651–3674, https://doi.org/10.1175/2009MWR2785.1.

Nolan, D. S., J. A. Zhang, and D. P. Stern, 2009b: Evaluation of planetary boundary layer parameterizations in tropical cyclones by comparison of in situ observations and high-resolution simulations of Hurricane Isabel (2003). Part II: Inner-core boundary layer and eyewall structure. *Mon. Wea. Rev.*, **137**, 3675–3698, https://doi.org/10.1175/2009MWR2786.1.

Ooyama, K. V., 1969: Numerical simulation of the life cycle of tropical cyclones. *J. Atmos. Sci.*, **26**, 3–40, https://doi.org/10.1175/1520-0469(1969)026<0003:NSOTLC>2.0.CO;2.

Rotunno, R., and K. A. Emanuel, 1987: An air-sea interaction theory for tropical cyclones. Part II: Evolutionary study using a nonhydrostatic axisymmetric numerical model. *J. Atmos. Sci.*, **44**, 542–561, https://doi.org/10.1175/1520-0469(1987)044<0542:AAITFT>2.0.CO;2.

Rotunno, R., and G. H. Bryan, 2012: Effects of parameterized diffusion on simulated

790 hurricanes. *J. Atmos. Sci.*, **69**, 2284–2299, https://doi.org/10.1175/JAS-D-11-0204.1.
791 Rotunno, R., Y. Chen, W. Wang, C. Davis, J. Dudhia, and G. J. Holland, 2009: Large-eddy
792 simulation of an idealized tropical cyclone. *Bull. Amer. Meteor. Soc.*, **90**, 1783–1788,
793 https://doi.org/10.1175/2009BAMS2884.1.
794 Stern, D. P., J. L. Vigh, D. S. Nolan, and F. Zhang, 2015: Revisiting the relationship between
795 eyewall contraction and intensification. *J. Atmos. Sci.*, **72**, 1283–1306, https://doi.org/
796 10.1175/JAS-D-14-0261.1.
797 Tao, D., M. Bell, R. Rotunno, and P. J. Van Leeuwen, 2020: Why do the maximum
798 intensities in modeled tropical cyclones vary under the same environmental conditions?
799 *Geophys. Res. Lett.*, **47**, e2019GL085980, https://doi.org/10.1029/2019gl085980.
800 Thompson, G., P. R. Field, R. M. Rasmussen, and W. D. Hall, 2008: Explicit forecasts of
801 winter precipitation using an improved bulk microphysics scheme. Part II:
802 Implementation of a new snow parameterization. *Mon. Wea. Rev.*, **136**, 5095–5115,
803 https://doi.org/10.1175/2008MWR2387.1.
804 Wang, W., B. Liu, L. Zhu, Z. Zhang, A. Mehra, and V. Tallapragada, 2021: A new horizontal
805 mixing-length formulation for numerical simulations of tropical cyclones. *Wea.*
806 *Forecasting*, **36**, 679–695, https://doi.org/10.1175/WAF-D-20-0134.1.
807 Wang, Y., 2002: Vortex Rossby waves in a numerically simulated tropical cyclone. Part
808 II: The role in tropical cyclone structure and intensity changes. *J. Atmos. Sci.,* **59**, 1239–
809 1262. https://doi.org/10.1175/1520-0469(2002)059<1239:VRWIAN>2.0.CO;2
810 Wood, V. T., and L. W. White, 2011: A new parametric model of vortex tangential-wind
811 profiles: Development, testing, and verification. *J. Atmos. Sci*., **68**, 990–1006,
812 https://doi.org/10.1175/2011JAS3588.1.
813 Wu, L., and S. A. Braun, 2004: Effect of convective asymmetries on hurricane intensity: A
814 numerical study. *J. Atmos. Sci.*, **61**, 3065–3081, https://doi.org/10.1175/JAS-3343.1.
815 Xu, J, and Y. Wang, 2010: Sensitivity of the simulated tropical cyclone inner-core size to the
816 initial vortex size. *Mon. Wea. Rev.*, **138**, 4135-4157,
817 https://doi.org/10.1175/2010MWR3335.1.
818 Zhang, J. A., F. D. Marks, M. T. Montgomery, and S. Lorsolo, 2011, An estimation of
819 turbulent characteristics in the low-level region of intense Hurricanes Allen (1980) and
820 Hugo (1989), *Mon. Wea. Rev.*, **139**, 1447–1462,
821 https://doi.org/10.1175/2010MWR3435.1.
822 Zhang, J. A., and M. T. Montgomery, 2012: Observational estimates of the horizontal eddy

823 diffusivity and mixing length in the low-level region of intense hurricanes, *J. Atmos. Sci.*,
824 **69**, 1306–1316, https://doi.org/10.1175/JAS-D-11-0180.1.
825 Zhang, J. A., and W. M. Drennan, 2012: An observational study of vertical eddy diffusivity
826 in the hurricane boundary layer. *J. Atmos. Sci.*, **69**, 3223–3236,
827 https://doi.org/10.1175/JAS-D-11-0348.1.
828 Zhang, J. A., and F. D. Marks, 2015: Effects of horizontal eddy diffusivity on tropical
829 cyclone intensity change and structure in idealized three-dimensional numerical
830 simulations. *Mon. Wea. Rev.*, **143**, 3981–3995, https://doi.org/10.1175/MWR-D-14-
831 00341.1.
832 Zhang, J. A., D. S. Nolan, R. F. Rogers, and V. Tallapragada, 2015: Evaluating the impact of
833 improvements in the boundary layer parameterizations on hurricane intensity and
834 structure forecasts in HWRF. *Mon. Wea. Rev.*, **143**, 3136–3154,
835 https://doi.org/10.1175/MWR-D-14-00339.1.
836 Zhang, J. A., F. D. Marks, J. A. Sippel, R. F. Rogers, X. Zhang, S. G. Gopalakrishnan, Z.
837 Zhang, and V. Tallapragada, 2018: Evaluating the impact of improvement in the
838 horizontal diffusion parameterization on hurricane prediction in the operational Hurricane
839 Weather Research and Forecast (HWRF) Model. *Wea. Forecasting*, **33**, 317–329,
840 https://doi.org/10.1175/WAF-D-17-0097.1.